CrossMark

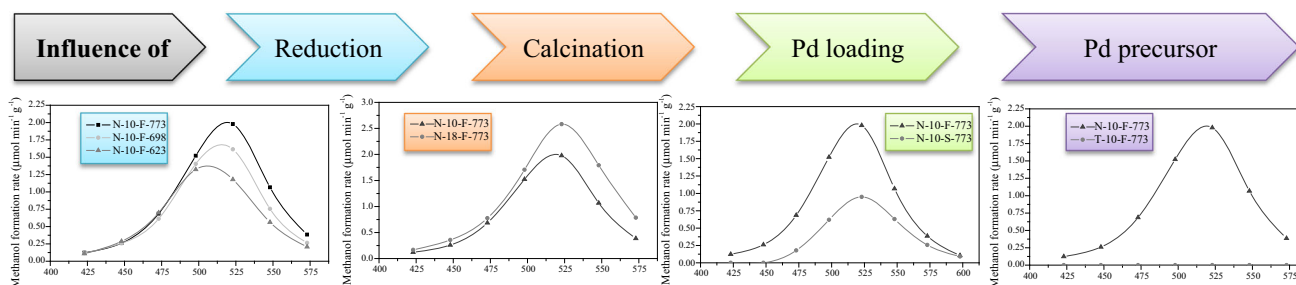# CO$_2$ Hydrogenation to Methanol at Atmospheric Pressure: Influence of the Preparation Method of Pd/ZnO Catalysts

J. Díez-Ramírez[1] · J. L. Valverde[1] · P. Sánchez[1] · F. Dorado[1]

Abstract The aim of the work described here was to evaluate the catalytic performance of palladium catalysts supported on zinc oxide (Pd/ZnO) in the hydrogenation of CO$_2$ to obtain methanol at atmospheric pressure. The influence of the reduction temperature, calcination conditions, metal loading and Pd precursor on the catalytic performance was studied.

Graphical Abstract

1 Introduction

The increase in atmospheric contamination and the desire to reduce the use of fossil fuels in recent decades have led to a search for alternative fuels to meet energy demands [1].

Hydrogen has been considered as a possible alternative fuel in recent years. However, the difficulties associated with the storage of hydrogen, along with the absence of energy distribution infrastructure and its low energy density for most practical applications, have severely limited the use of hydrogen [2]. However, it can be used as a promising energy carrier, as it could be transformed into other compounds. Methanol represents one way to store hydrogen in the liquid state and this overcomes the problems outlined above. Methanol is frequently used as solvent and feedstock for chemicals production. Furthermore, it could be used like an alternative fuel in the energy distribution infrastructure that exists nowadays, or it can also be blended with gasoline [3]. Methanol is therefore one of the alternative fuels that is widely studied by the scientific community [4].

✉ J. Díez-Ramírez
javier.diez@uclm.es

[1] Departamento de Ingeniería Química, Facultad de Ciencias y Tecnologías Químicas, Avenida Camilo José Cela 12, 13005 Ciudad Real, Spain

At present, most commercial methanol is produced from synthetic gas or syngas (H_2 and CO), which is obtained by catalytic reforming of fossil fuels [3]. Nevertheless, the real scientific target is to replace carbon monoxide with carbon dioxide, as shown in Eq. (1), and to obtain good conversion and selectivity towards methanol [5].

$$CO_2 + 3H_2 \rightarrow CH_3OH + H_2O \qquad (1)$$
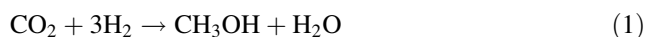
On the one hand, the use of carbon dioxide for the production of methanol is one of the ways in which value can be added to this pollutant, which is closely associated with the greenhouse effect. Carbon dioxide would be captured by different methods and this would decrease the levels of this pollutant in the atmosphere [6]. On the other hand, the use of hydrogen in that reaction limits the economy of the process, but it could change if the hydrogen is produced by (for instance) the hydrolysis of water, which is an abundant component in nature, and the energy required for the hydrolysis is obtained from renewable sources like solar or wind power [7]. Accordingly, the methanol produced could be considered as a 'green fuel' because it would be obtained from renewable energy and the net balance of carbon dioxide in the atmosphere is not increased if the methanol production utilizes more CO_2 than that produced in the manufacture of H_2 [8].

Despite the fact that methanol synthesis has been widely studied, in most references in the literature this reaction is carried out at high pressure [8–11]. Studies carried out at atmospheric pressure are scarcer [12, 13] and in-depth studies of the preparation steps for the catalysts employed for the reaction have not been described. In the work reported here, the hydrogenation of CO_2 to methanol over Pd/ZnO catalysts at atmospheric pressure was carried out. This catalyst was selected because it is well known to give good performance in this reaction. The influence of the calcination and reduction steps, the metal loading and the Pd salt precursor on the catalytic activity were studied.

2 Experimental

2.1 Catalyst Preparation

Catalysts were prepared by the wet impregnation method using ZnO (Panreac) as the support and palladium(II) nitrate [Pd(NO$_3$)$_2$·xH$_2$O, Aldrich] or tetraamminepalladium(II) nitrate [Pd(NH$_3$)$_4$(NO$_3$)$_2$, Aldrich] as precursors, with the appropriate quantities added to an aqueous solution in order to obtain catalysts with a Pd load of 10 or 15 wt%. After impregnation, the catalysts were dried at 393 K overnight. Two different methods were used for the calcination step. The 'slow calcination' was carried out in a tubular reactor (75 cm length divided at the middle into

two parts with two different diameters, 1.5 and 0.7 cm, respectively) under an air stream (333 mL/min). The temperature was first increased to 453 K at a heating rate of 1.3 K/min and then held at this temperature for 2 h before being increased again up to 773 K, at the same heating rate, and then held for a further 2 h. The 'fast calcination' was carried out in an oven under static air at 773 K for 3 h at a heating rate of 5 K/min. Finally, a reduction step was carried out prior to reaction and this is discussed in Sect. 2.3. The catalysts were denoted as X-number1-Y-number2, where X indicates the precursor palladium(II) nitrate (N) or tetraamminepalladium(II) nitrate (T), number1 the metal loading, Y the calcination method, fast (F) or slow (S), and number2 the reduction temperature. For ease of reference the preparation conditions and nomenclature of the samples are summarized in Table 1.

2.2 Catalyst Characterization

Pd metal loading was determined by atomic absorption (AA) spectrophotometry on a SPECTRA 220FS analyser. Samples (ca. 0.5 g) were treated with 2 mL HCl, 3 mL HF and 2 mL H_2O_2 followed by microwave digestion (523 K). Surface area/porosity measurements were carried out using a QUADRASORB 3SI sorptometer apparatus with N_2 as the sorbate at 77 K. The samples were outgassed at 523 K under vacuum (5×10^{-3} Torr) for 12 h prior to analysis. Specific surface areas were determined by the multi-point BET method. Specific total pore volume was evaluated from N_2 uptake at a relative pressure of P/Po = 0.99. Temperature-programmed reduction (TPR) experiments were conducted in a commercial Micromeritics AutoChem 2950 HP unit with TCD detection. Samples (ca. 0.15 g) were loaded into a U-shaped tube and ramped from room temperature to 973 K (10 K/min), using a reducing gas mixture of 17.5 % v/v H_2/Ar (60 cm^3/min). The same unit was used to measure the metal dispersion. Catalysts (150 mg) were typically purged with dry helium at 100 °C for 1 h and then reduced in 17.5 % v/v H_2/Ar (25 cm^3/min) at 773 K for 3 h. Subsequently, the sample was cooled down to room temperature and exposed to pulses of H_2 until five consecutive pulses yielded identical signal areas. XRD analyses were conducted with a Philips X'Pert instrument using nickel-filtered Cu-Kα radiation. Samples were scanned at a rate of 0.02° step^{-1} over the range $5° \leq 2\theta \leq 90°$ (scan time = 2 s step^{-1}). Transmission electron microscopy (TEM) analyses were conducted on a JEOL JEM-4000EX unit with an accelerating voltage of 400 kV. Samples were prepared by ultrasonic dispersion in acetone with a drop of the resulting suspension evaporated onto a holey carbon-supported grid. The instrument was equipped with an energy dispersive X-ray spectroscopy (EDS) unit. Saturation was assumed to be complete after

Table 1 Nomenclature and preparation method of the samples

Precursor	Metal loading (%)	Calcination step	Reduction temperature (K)	Nomenclature
Palladium (II) nitrate	10.9	Fast calcination	623	N-10-F-623
			698	N-10-F-698
			773	N-10-F-773
		Slow calcination	773	N-10-S-773
	18.1	Fast calcination	773	N-18-F-773
Tetraamminepalladium(II) nitrate	9.9	Fast calcination	773	T-10-F-773

three successive peaks showed the same peak areas. Thermogravimetric analysis was carried out on a TGA apparatus (TGA-DSC 1, Mettler Toledo). The sample was heated from ambient to 1000 K at 10 K/min under a reactive atmosphere of 21 % of oxygen and 79 % nitrogen. The TG curve represents the evolution of the mass as a function of temperature.

2.3 Catalyst Activity Measurement

Experiments were carried out in a tubular quartz reactor (45 cm length and 1 cm diameter). The catalyst, with a particle size in the range 250–500 μm and without dilution, was placed on a fritted quartz plate located at the end of the reactor. The temperature of the catalyst was measured with a K-type thermocouple (Thermocoax) placed inside the inner quartz tube. The entire reactor was placed in a furnace (Lenton) equipped with a temperature-programmed system. Reaction gases were Praxair certified standards of CO$_2$ (99.999 % purity), H$_2$ (99.999 % purity) and N$_2$ (99.999 % purity). The gas flows were controlled by a set of calibrated mass flowmeters (Brooks 5850 E and 5850 S).

Prior to the reaction, catalysts (0.8 g) were reduced in situ in a hydrogen stream (10 vol%) diluted with nitrogen at a flow rate of 25 cm^3/min. The temperature was increased at a heating rate of 1.3 K/min up to different final values, as shown in Table 1. The reduction step was finished once the final reduction temperature was reached. The reaction was then carried out at atmospheric pressure in the temperature range 423–573 K. The total flow rate, which was a CO$_2$/H$_2$ mixture (CO$_2$/H$_2$ = 1/9), was maintained at 100 cm^3/min. Gas effluents were monitored by a micro gas chromatograph (Varian CP-4900).

3 Results and Discussion

3.1 Influence of the Reduction Temperature

The XRD patterns for different samples, before and after reduction, are shown in Fig. 1. Prior to reduction (Fig. 1a) the main diffraction peaks corresponded to ZnO and PdO.

After reduction (Fig. 1b), the PdO peaks disappeared and new diffraction peaks (around 2θ = 41.22° and 44.14°) were found and these are assigned to PdZn alloys. It can be observed that higher reduction temperatures led to a higher intensity for these new peaks, indicating that the formation of crystalline PdZn alloys is favored by higher reduction temperatures. Methanol production takes place on PdZn alloy sites, whereas CO is selectively produced on metallic Pd [12]. The methanol, CO and CH$_4$ activities at different temperatures are represented in Fig. 2. The catalytic results were consistent with the XRD patterns. CH$_4$ and CO activity increased when the catalyst was reduced at a lower temperature (more metallic Pd and less PdZn alloys), whereas methanol formation was favored by a higher reduction temperature. The selectivity to methanol at the same CO$_2$ conversion level ($\sim$4 %) was 15.7, 8.3 and 6.9 % for the N-10-F-773, N-10-F-698 and N-10-F-623 samples, respectively. It shows that a major quantity of PdZn alloy provides a higher selectivity. It should be noted that, even though the catalytic experiments were carried out under atmospheric pressure, the results are far away from the thermodynamic equilibrium values, showing that there are not thermodynamic limitations (see Table 2). The thermodynamic equilibrium values were calculated using a flowsheet simulator (Aspen HYSYS V8.4 licensed by Aspen Technology,Inc.). Peng Robinson was used as the equation of state and the reactor modeling was based on a Gibbs reactor. The conditions used for the simulation (flow rate, CO$_2$/H$_2$ ratio) were the same as in the experimental reactor.

3.2 Influence of the Calcination Conditions

The catalyst N-10 was calcined using two different methods, slow and fast, as described in Sect. 2.1. It should be noted that the calcination temperature was chosen based on thermogravimetric (TG) analysis of the N-10 sample (Fig. 3). The marked weight loss at around 400–500 K is due to the removal of the water absorbed during the impregnation step and to decomposition of the nitrate precursor. The sample is stable in the range 700–1000 K. Therefore, for the slow method, an initial step was carried

Fig. 1 XRD profiles of **a** N-10-F catalyst before reduction, where (*cap symbol*) denotes reflection of ZnO and (*degree symbol*) denotes reflection of PdO. **b** N-10-F-623, N-10-F-698 and N-10-F-773. **c** N-10-F-773 and N-10-S-773. **d** N-10-F-773 and N-15-F-773 catalysts
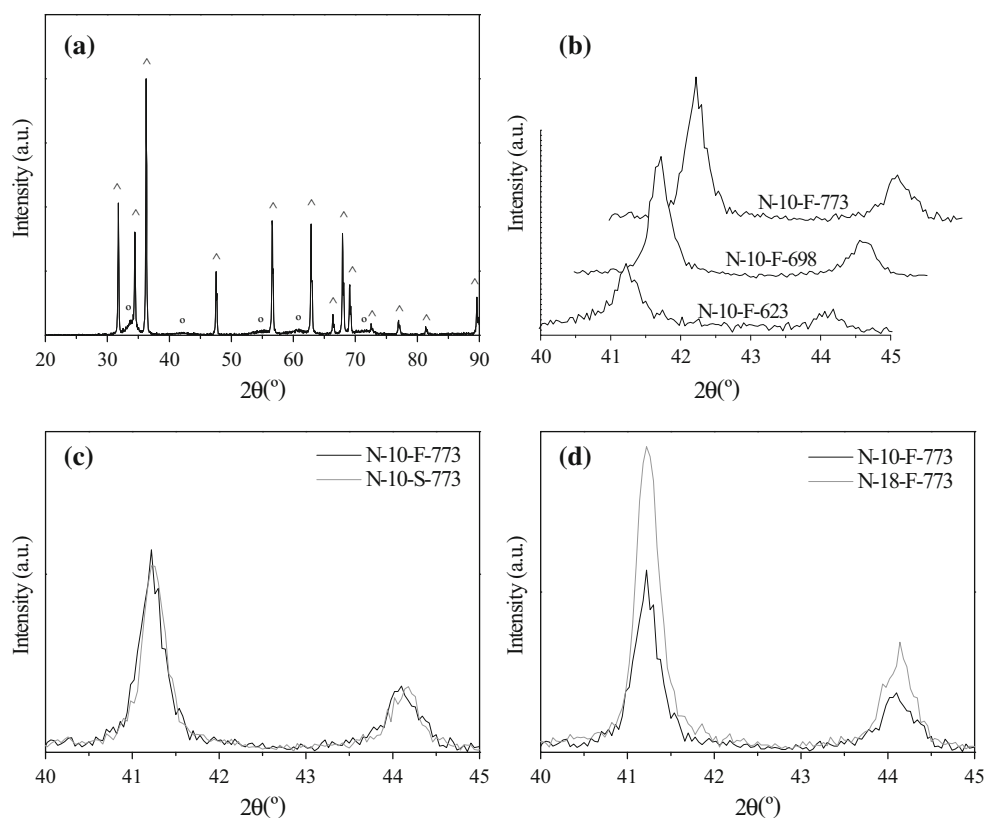

out at 453 K to allow a gradual loss of water and decomposition of the metal precursor, and a second step was then performed at 773 K, i.e., the maximum reduction temperature at which the sample is still stable.

The XRD profiles of samples obtained by the two calcination methods (Fig. 1c) were not significantly different. However, interestingly, the catalytic results (Fig. 4) showed very clear differences between the two samples. The CO_2 conversion was higher for the sample N-10-S-773, although consequently the selectivity to methanol decreased. At the same CO_2 conversion level ($\sim$7.8 %), the selectivity to methanol was of 0.95 and 0.77 % for the N-10-F-773 and N-10-S-773 samples, respectively. Therefore, the methanol formation rate was higher for the sample obtained by fast calcination, whereas the CO and CH_4 activities were lower. Thus, PdZn alloy formation is not the only parameter that affects the catalytic performance. In an effort to understand this result, the catalysts were characterized in more depth. The surface properties of the materials are given in Table 3. Surface area and pore volume are slightly higher for the sample obtained by slow calcination, probably due to a different morphology created during the calcination step. This change in the support morphology could be due to the faster kinetic of the support degradation during the fast calcination. This degradation is caused by the metal precursor, which can dissolve the ZnO (due the acidity of the metal nitrate aqueous

solution [14]). It would explain the different ZnO crystal size for the N-10-F-773 and N-10-S-773 samples (98 and 189 nm, respectively).

Moreover, metal dispersion is somewhat higher for the sample obtained by slow calcination. These results are consistent with the TEM pictures (Fig. 5a, b). The smallest particles found in the TEM images correspond to metallic Pd, whereas the largest particles are assigned to PdZn alloys. It must be noted that the TEM particle sizes shown in Table 3 were measured by taking into account all Pd particles, i.e., without distinguishing between metallic Pd and PdZn alloys. As in previous studies [15], the Pd was found to be dispersed on the ZnO matrix with an average particle size of around 4 nm. It should be noted that the peaks corresponding to metallic Pd did not appear in the XRD profiles for two reasons: (i) the amount of Pd^0 is less than 1 wt% and (ii) these particles are smaller than 2 nm, which is beyond the detection limit of XRD. Energy dispersive X-ray microanalysis (Table 4) was carried out to demonstrate that the large particles correspond to PdZn alloys. Analysis in region A detected Pd and Zn in similar quantities and this is related to the presence of PdZn alloys. Region B showed only Zn and this was therefore assigned to the ZnO support. The TEM images showed that smaller particles were present in the catalyst calcined by the slow method. This means that there was more metallic Pd, which is consistent with the higher CO and methane production
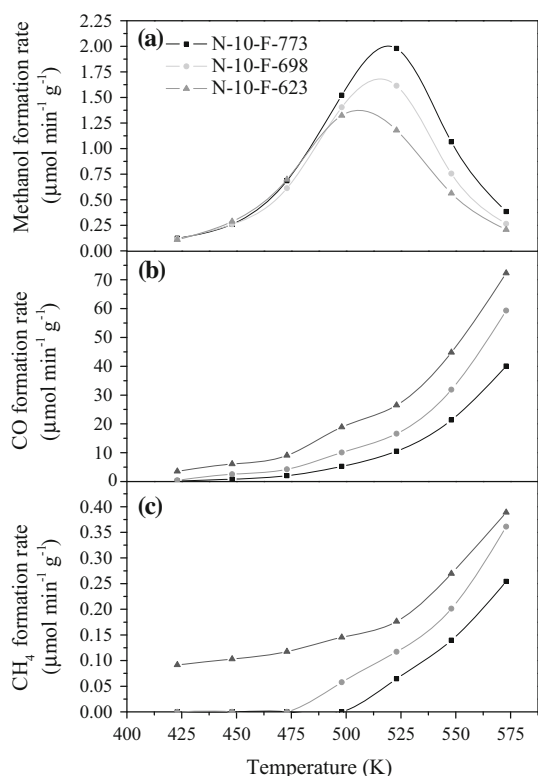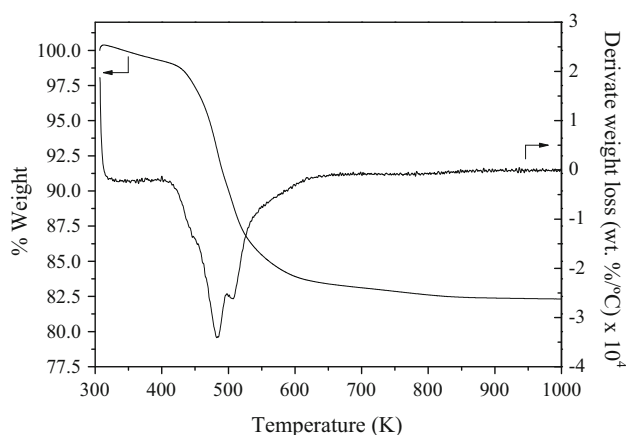
Fig. 2 Catalytic activity for N-10-F-623, N-10-F-698 and N-10-F-773. Formation rates of **a** methanol **b** CO and **c** CH$_4$. Reaction conditions: CO$_2$/H$_2$ = 1/9 and W/F = 0.008 g min/cm^3
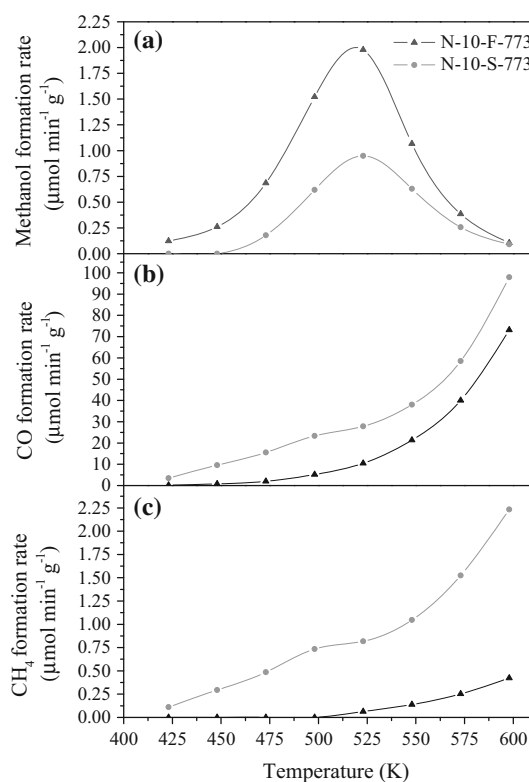
Table 2 Comparison between thermodynamic equilibrium and experimental values for the catalyst N-10-F-773

Temperature (K)	Thermodynamic (µmol/min)	Experimental (µmol/min)
423	22.24	0.10
448	14.72	0.21
473	10.09	0.55
498	7.14	1.22
523	5.19	1.58
548	3.87	0.85

Fig. 3 Thermogravimetric profile of N-10 catalyst

Fig. 4 Catalytic activity for N-10-F-773 and N-10-S-773. Formation rates of **a** methanol **b** CO and **c** CH$_4$. Reaction conditions: CO$_2$/H$_2$ = 1/9 and W/F. = 0.008 g min/cm^3

observed. Moreover, the N-10-S-773 catalyst showed in XRD and TEM analysis smaller particle size for the PdZn alloy particles that has previously been correlated with higher CO selectivity in the steam reforming of methanol [16, 17]. The metal particle distribution (Fig. 5f) was also in agreement with this result. Both catalysts showed a Gaussian particle distribution, but for the slow calcination method this was shifted to the left. Therefore, the Pd particles in this catalyst, related to the smaller particles in the Gaussian distribution, were found in major proportion than those obtained for the fast calcination. In addition, the particles related to the formation of PdZn alloys (bigger

particles) and, consequently, to the higher methanol production rate were detected in a lesser proportion when the slow calcination method was employed. For instance, for the N-10-F-773 sample, the 8.6 % of the particles were larger than 25 nm. This effect could be due to an easier mobility of the palladium cations. When the metal is loaded, it is surrounded by H$_2$O ligands coming from the aqueous solution. These ligands are removed during the

Table 3 Main physical properties of the catalysts

	N-10-F	N-10-S	N-18-F	T-10-F
Surface Area (m^2/g)	8.6	9.5	7.1	7.5
Total pore volume (cm^3/g) $\times 10^2$	3.4	5.5	3.6	4.1
Dispersion (%)	1.47	1.59	0.82	0.34
Particle diameter PdZn from XRD (nm)	60.8	50.3	77.1	33.4
Particle diameter Pd^0 from XRD (nm)	–	–	–	63.9
Particle diameter ZnO from XRD (nm)	98	189	–	–
Particle diameter from TEM (nm)	22.1	14.9	28.4	71.6

calcination step, and logically the faster heating rate, the easier the ligands removal. When the metal becomes "bared", it can migrate to more stable positions [18]. It could explain the formation of bigger particles of PdZn alloy.

TPR profiles obtained from room temperature to 973 K for these two catalysts are shown in Fig. 6a. The two profiles are quite similar. The inverse peak found at around 320 K is assigned to PdH$_x$ decomposition to give metallic Pd. According to the literature [19, 20], when hydrogen is fed over the catalyst at room temperature, hydrogen consumption occurs rapidly and PdO is partially converted to PdH$_x$ [15]. This peak in hydrogen consumption was not observed in our profiles, as hydrogen is in contact with the catalyst before the TPR experiment starts. Interpretation of the peaks above 600 K is not trivial, although they are commonly related to crystalline PdZn alloy formation [15, 19, 20]. The two peaks at around 600 and 750 K could be assigned to the different changes in the Pd/ZnO crystal structure during the reduction process [21], where the Pd/ZnO structure is modified in different steps as follows: PdO/ZnO → Pd/ZnO → PdZnO1–x/ZnO → amorphous PdZn alloy/ZnO → crystalline PdZn alloy/ZnO.

3.3 Influence of the Metal Loading

In order to study the influence of the metal loading, two samples (N-10-F-773 and N-18-F-773) with different metal contents were compared. The catalytic activities obtained for these samples are shown in Fig. 7. As expected, the methanol formation rate increased with the metal loading as there was more Pd available to form PdZn alloys. This result is consistent with the XRD profiles obtained for these samples (Fig. 1d), where the main peaks corresponding to PdZn alloys were much more intense for the sample with a higher metal loading. Moreover, an increase in the metal loading improved the selectivity to methanol, as shown in Fig. 7d. A methanol selectivity of 100 % was obtained for the catalyst with a metal content of 18 % at 425 K.

The main physical properties of these catalysts can be compared from the data in Table 3. The N-10-F-773 catalyst surface area was higher than that of the ZnO support

(7.0 m^2 g^{-1}). However, the surface area was lower for the N-18-F-773 sample. Similar behavior has been described in the literature [14]. As commented above, it is caused by dissolution of the support (ZnO) during the impregnation of Pd, so that the textural properties (porosity and crystal structure of ZnO) are modified. When the metal content was increased, the Pd was distributed in such a way that larger particles or alloys were formed, thus increasing the volume of the particles and reducing the surface area of the catalyst. This situation was confirmed by the lower metal dispersion found in the catalyst with a higher metal loading. The TEM pictures and the corresponding metal particle distribution were also in agreement with this situation. Large PdZn alloy particles were found in the N-18-F-773 sample (Fig. 5c). The percentage of particles greater than 25 nm for this catalyst was 10.7 %, whereas the value for the N-10-F-773 sample was 8.6 %.

TPR profiles for these samples are shown in Fig. 6b. As mentioned in the previous section, the catalyst with a 18 % metal loading had a lower quantity of metallic palladium, which is related to the inverse peak at 325 K, and more crystalline PdZn alloys related to the peak at 750 K.

The low quantity of available metallic Pd would explain the poor methanation activity, whereas the higher quantity of PdZn alloys is responsible for the increase in methanol production. However, it should be noted that even though there were more PdZn alloy particles for the catalysts with a higher metal content, they were also larger and a proportion of the Pd was inaccessible as it was trapped inside these particles. Thus, if the methanol formation rate is calculated in terms of TOF (turnover frequency) to take into account the available Pd sites, better results were obtained for the N-10-F-773 catalyst (Fig. 7e), indicating that the loss of available Pd sites is not compensated by the extra metal load.

3.4 Influence of the Precursor

The performance levels of two catalysts (N-10-F-773 and T-10-F-773) prepared with different precursors were compared. The catalytic results are represented in Fig. 8.
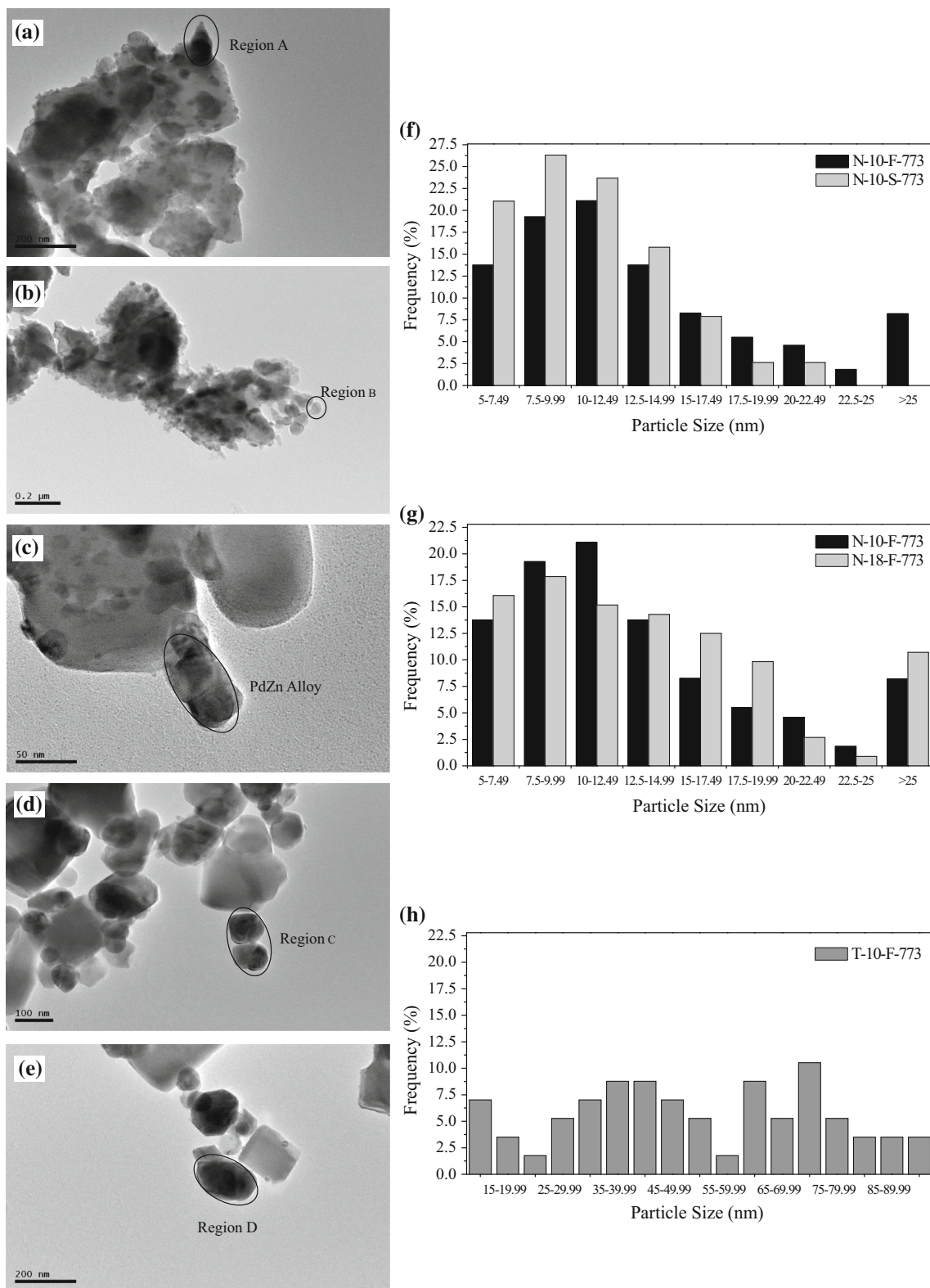
Fig. 5 High resolution TEM and metal particle distribution on **a** N-10-F-773. **b** N-10-S-773. **c** N-15-F-773 and **d**, **e** T-10-F-773. **f** N-10-F-773 and N-10-S-773. **g** N-10-F-773 and N-15-F-773. **h** T-10-F-773

Table 4 Energy dispersive X-ray microanalysis results of region A, B, C and D from Fig. 5

Element	Weight (%)			
	Region A	Region B	Region C	Region D
Zn	57.70	99.7	47.54	31.97
Pd	42.30	0.3	52.46	68.03

As observed, the activity for the T-10-F-773 sample was almost negligible.

The XRD profiles for the two catalysts before and after the reduction step are shown in Fig. 9. There are some interesting differences between the two precursors. Before reduction of the N-10-F-773 sample, only the peaks assigned to the support and the palladium oxide were observed. However, for the T-10-F-773 sample the peaks
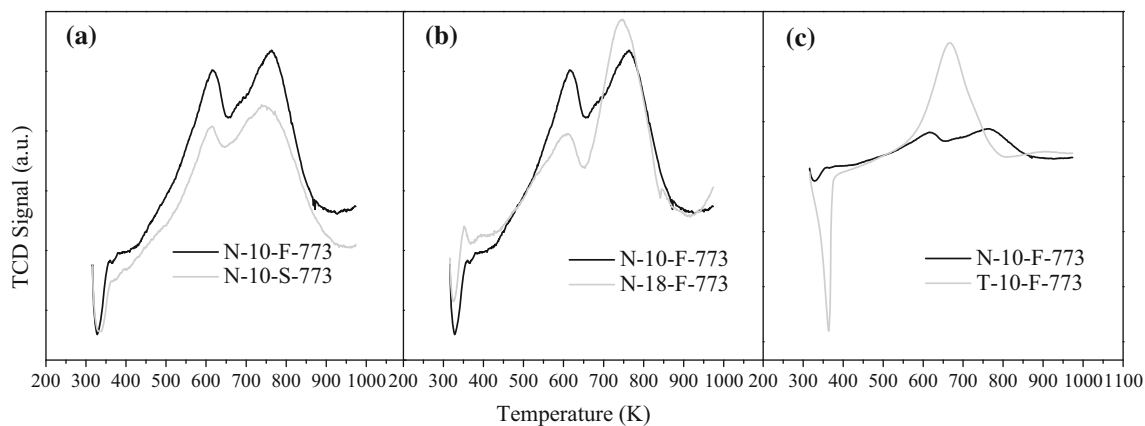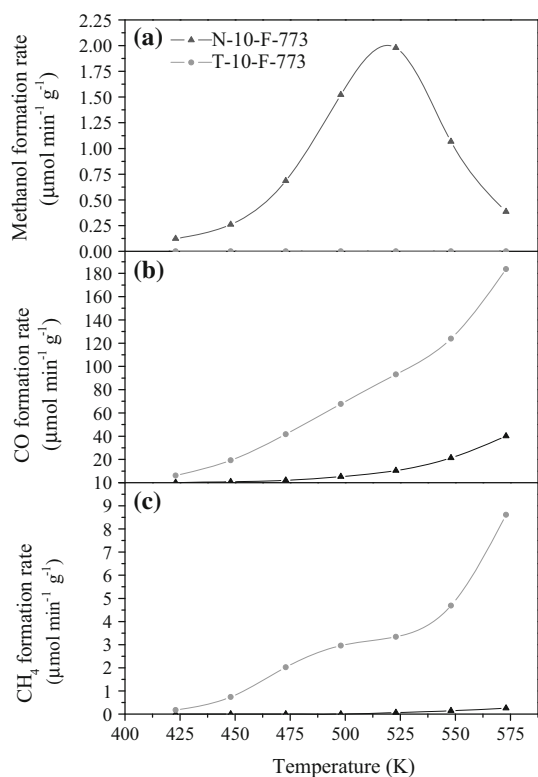

Fig. 6 TPR profiles. Comparison between **a** N-10-F and N-10-S. **b** N-10-F and N-15-F and **c** N-10-F and T-10-F
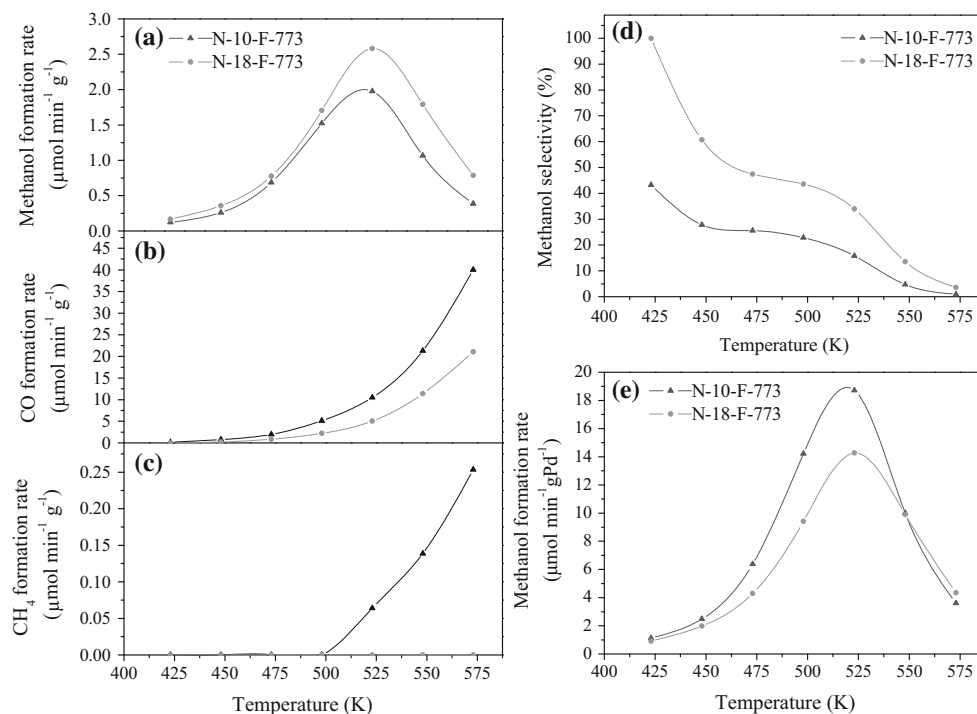
Fig. 7 Catalytic activity for N-10-F-773 and N-15-F-773. Formation rates of **a** methanol **b** CO and **c** CH_4 **d** methanol selectivity and **e** methanol activity calculated per gram of Pd metal on the catalyst for the different metal loadings. Reaction conditions: $CO_2/H_2 = 1/9$ and $W/F = 0.008$ g min/cm^{-3}
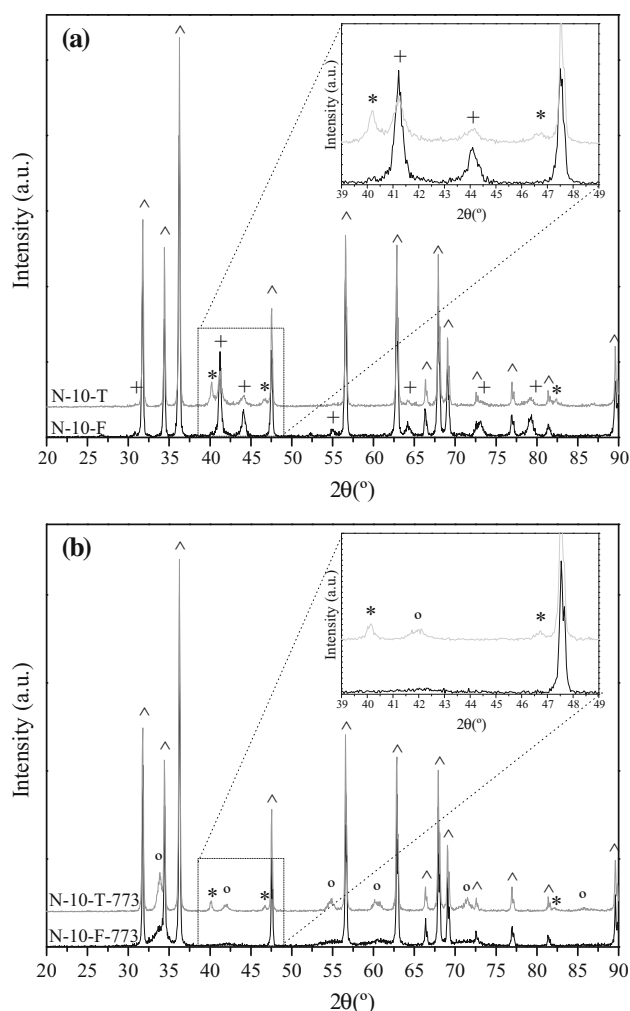
assigned to metallic palladium were also observed. For this catalyst, the NH_3 formed by degradation of the salt during the calcination step was able to reduce the palladium, as it is well known [18]. After reduction, the peaks assigned to PdZn alloys were observed for both samples, but they were rather less intense for the T-10-F-773 catalyst, for which the signal corresponding to metallic palladium was still observed.

The TEM pictures for the latter sample are shown in Fig. 5d, e. It can be clearly observed that the morphology of the particles changes completely when compared to the other catalysts (much larger particles were detected). Energy dispersive X-ray microanalysis was carried out to measure the element contents in the two characteristic regions (C and D) for the T-10-F-773 sample (Table 4). The larger particles would correspond to PdZn alloys (region C, where the metal contents of Zn and Pd are very close) and to metallic palladium deposited on the ZnO matrix (region D, where the palladium content is higher than that of zinc). This situation is also consistent with the XRD profile of this catalyst, in which the peaks for both species' were detected. The formation of metallic Pd during the calcination step and its subsequent sintering during the reduction step would explain the formation of the large Pd^0 particles. In any case, the metal particle distribution for

Fig. 9 XRD profile **a** before reduction and **b** after reduction of N-10-F-773 and T-10-F-773, where (*cap symbol*) denotes reflection of ZnO, (*degree symbol*) denotes reflection of PdO, (*plus sign*) denotes reflection of PdZn alloys and (*asterisk*) denotes reflection of metallic palladium

Fig. 8 Catalytic activity for N-10-F-773 and T-10-F-773. Formation rates of **a** methanol **b** CO and **c** CH₄. Reaction conditions: CO₂/H₂ = 1/9 and W/F = 0.008 g min/cm³

the T-10-F-773 sample (Fig. 5h) showed a high degree of heterogeneity and particles of various different sizes were found. An average particle size obtained from the XRD patterns and TEM images is given in Table 3. In agreement with the previous results, the metallic Pd particles showed a much higher value than those determined for the other catalysts.

The TPR profile for this sample is shown in Fig. 6c. This profile is completely different to those obtained for the other samples. There is a large inverse peak and this confirms the high quantity of metallic palladium. After this, only a single peak at around 650 K is observed. The second peak found for the other catalysts at 750 K was not detected for this sample, which suggests that the evolution from PdO/ZnO to a crystalline PdZn alloy/ZnO is incomplete and that very little of the latter species is formed.

Therefore, for the T-10-F-773 there are smaller PdZn alloy particles and most of these are amorphous and inactive to methanol production, meaning that methanol is not obtained. In addition, the presence of larger metallic Pd particles leads to higher CO and CH_4 production.

4 Conclusions

The following conclusions can be drawn from this study:

– The reduction temperature has a marked effect on the distribution of the species that are formed. A higher reduction temperature leads to the formation of more PdZn alloy particles. These alloy particles are directly related to a major conversion towards methanol. Hence, an increase in the reduction temperature improves the reaction rate and selectivity to methanol.
– The calcination conditions are important to control how particles are formed. Smaller particles of metallic palladium were found after a slow calcination. These particles are related to CO production and they decrease methanol selectivity and production.
– A higher metal loading leads to higher methanol production as more PdZn alloy particles are formed. However, the TOF is lower as these new particles are bigger and the dispersion is poor.
– The precursor used to load the Pd has a marked influence on the final catalyst structure. When tetraamminepalladium(II) nitrate was used, the ammonia formed by salt degradation reduced the metal during the calcination step. Hence, during the reduction step there is strong metal sintering. Numerous metallic Pd particles, which have a large size, are obtained and the formation of PdZn alloy particles is hindered. As a consequence, methanol production is suppressed.

References

1. Guo KW (2013) Fossil fuels: sources, environmental concerns and waste management practices. Nova Science Publishers, New York, pp 85–99
2. Strahan D (2008) New Sci 200:40–43
3. Olah GA (2005) Angew Chem Int Ed 44:2636–2639
4. Bockris JO (2008) Int J Hydrogen Energ 33:2129–2131
5. Ganesh I (2014) Renew Sust Energ Rev 31:221–257
6. Spigarelli BP, Kawatra SK (2013) J CO2 Util 1:69–87
7. Raudaskoski R, Turpeinen E, Lenkkeri R, Pongrácz E, Keiski RL (2009) Catal Today 144:318–323
8. Jadhav SG, Vaidya PD, Bhanage BM, Joshi JB (2014) Chem Eng Res Des 92:2557–2567
9. Ban H, Li C, Asami K, Fujimoto K (2014) Catal Commun 54:50–54
10. Liang XL, Xie JR, Liu ZM (2015) Catal Lett 145:1138–1147
11. Lei H, Nie R, Wu G, Hou Z (2015) Fuel 154:161–166
12. Iwasa N, Suzuki H, Terashita M, Arai M, Takezawa N (2004) Catal Lett 96:75–78
13. Maniecki TP, Mierczynski P, Maniukiewicz W, Bawolak K, Gebauer D, Jozwiak WK (2009) Catal Lett 130:481–488
14. Chin YH, Wang Y, Dagle RA, Li XS (2003) Fuel Process Technol 83:193–201
15. Chin YH, Dagle R, Hu J, Dohnalkova AC, Wang Y (2002) Catal Today 77:79–88
16. Zhang H, Sun J, Dagle VL, Halevi B, Datye AK, Wang Y (2014) ACS Catal 4:2379–2386
17. Dagle RA, Chin YH, Wang Y (2007) Top Catal 46:358–362
18. Sachtler WMH, Zhang Z (1993) Adv Catal 39:129–220
19. Iwasa N, Mayanagi T, Ogawa N, Sakata K, Takezawa N (1998) Catal Lett 54:119–123
20. Iwasa N, Masuda S, Ogawa N, Takezawa N (1995) Appl Catal A Gen 125:145–157
21. Wang Y, Zhang J, Xu H (2006) Chin J Catal 27:217–222